On the efficiency of parallel baffle-type silencers in rectangular ducts: prediction and measurement

R. Binois, E. Perrey-Debain, N. Dauchez, Benoit Nennig, J.-M. Ville, G. Beillard

On the efficiency of parallel baffle-type silencers in rectangular ducts: prediction and measurement

R. Binois[1,2,3)], E. Perrey-Debain[,1)], N. Dauchez[,1)], B. Nennig[,2)], J.-M. Ville[1)] and G. Beillard[3)]

[1)]Laboratoire Roberval UMR 7337, Centre de Recherches de Royallieu,
Université de Technologie de Compiègne (UTC),
CS 60319, 60203 Compiègne cedex, France.
[2)]Laboratoire d'Ingénierie des Systèmes Mécaniques et des Matériaux
EA 2336 (Quartz - LISMMA), Institut Supérieur de Mécanique de Paris,
3 rue Fernand Hainaut, 93400 Saint-Ouen, France.
[3)]Alhyange Acoustique, 60 rue du Faubourg Poissonnière,
75010 Paris, France.

Preprint submitted to *acta acustica united with acustica*, 2015

Abstract

To estimate the efficiency of parallel baffle-type silencers in rectangular ducts, a two-dimensional multi-layer model is presented for predicting their transmission loss. The approach takes into account an arbitrary number of bulk reacting baffles of finite length bounded at both ends by a metallic fairing. Each layer is described by a mean pressure, which allows computing a piecewise constant modal basis for the mean pressure over the cross section. The continuity between the incoming and outgoing waves is performed by axial mode matching at the inlet and outlet cross-sections of the baffle silencer. It is shown that the model is easy to implement and suitable for optimization purposes based on design parameters such as the height of each baffle, their relative positions in the duct, and material properties. Relatively complex configurations can be simulated with relatively modest computational effort. An experimental campaign was carried out on a reduced scale test bench for standard configurations. The numerical results are in good agreement with the measurements. Noise reduction performances are analyzed in terms of reflected and dissipated sound powers. Finally, more complex geometric configurations are simulated in order to examine the influence of the relative transverse and axial positions of each baffle as well as the effect of a resistive screen between the baffles and the airways.

1 Introduction

Baffle-type silencers are widely used in the heating, ventilation and air conditioning (HVAC) systems of buildings to reduce noise being emitted from air-moving devices such as fans and air conditioners. These silencers generally consist of several baffles inserted in a duct with a rectangular cross section (see for instance Fig. 1). Each baffle is made of sound absorbing material such as rockwool or glasswool. The presence of air flow inside the HVAC duct leads to the use of thin veils or perforated metal sheets between the baffles and the airways for protection. Usually, a metallic fairing is also placed at each end of the baffle.

The analysis of sound propagation through dissipative silencers is generally performed using classical dicretization techniques such as the very popular Finite Element Method (FEM) [1, 2, 3, 4, 5]

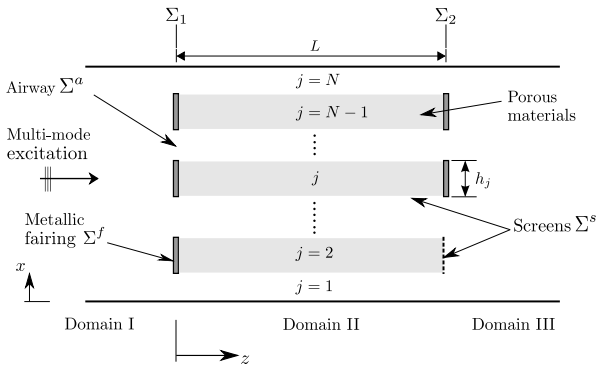

Figure 1: Plan view of typical parallel-baffle silencer geometry.

and the Boundary Element Method (BEM) [6]. Although these methods can be used to model a large variety of geometrical configurations, they are known to be demanding, both in terms of data preparation and computation, rendering optimization procedures somewhat cumbersome. Another approach that takes advantage of the axially invariant properties of these types of silencer consists in expanding the acoustic field as a truncated sum over the silencer eigenmodes. This modal approach is attractive because it immediately reduces the dimension of the problem, i.e. only the acoustic eigenmodes over the cross-section of the silencer must be calculated, which can be much quicker than using a full FEM model. Regarding the specific case of parallel baffle-type silencers, three variants of the modal approach stand out in the scientific literature: (i) Ko [7], and Cummings & Sormaz [8] obtained eigenmodes analytically by using appropriate root-finding algorithms. However, the geometrical assumption that the silencer is of infinite length restricted their analysis to the prediction of modal attenuations only. (ii) In the specific case where baffles are arranged periodically, Mechel [9, 10], and Tam and Fahy [11], determined the modal sound field in the silencer section analytically. A mode matching method was then applied to quantify the scattering effects over the inlet and outlet planes of the silencer, for transmission loss and sound intensity, respectively. (iii) In order to address more general configurations, Kirby [12] performed a finite element eigenvalue analysis and axial mode matching to calculate the transmission loss of baffle-type silencers with metallic fairings. He underlined the fact that at low frequencies, the effect of the silencer geometry predominates and that a two-dimensional model is sufficient for evaluating silencer performance.

The present paper proposes an easy-to-implement and relatively inexpensive numerical multi-layer model tailored specifically for analyzing the performances of parallel baffle-type silencers. It can simulate a wide variety of configurations and is suitable for optimization purposes based on design parameters such as the height of each baffle, their relative positions in the duct, and material properties. The model can be considered as an extension of the low-frequency model developed by Aurégan *et al.* [13] for a coaxial cylindrical dissipative silencer. It is similar to classical FEM eigenmode analysis except that the mean pressure across each layer, i.e. the baffle or the airway, is used as a degree of freedom instead of the nodal pressure value. This renders the axial mode matching procedure considerably easier. The consideration of a resistive screen between an airway and a porous material layer is also facilitated.

The present paper is organized as follows. First the geometry and the assumptions for the problem are defined. The main ingredients of the method, namely the modal basis for the mean pressure and the mode matching procedure are then presented with all the necessary details. Thereafter, the experimental setup is explained and the numerical results are compared against new experimental data for two standard geometric configurations. The performance of both standard silencers are analyzed in terms of reflected and dissipated sound powers. Finally, the method is applied to the simulation of two other configurations with more complex geometries and several results are presented and discussed.

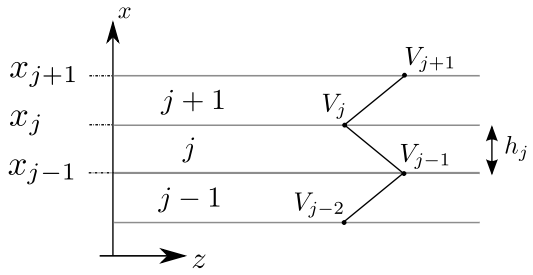

Figure 2: Transverse velocity profile.

2 Silencer model

Without loss of generality, we present our numerical model for the analysis of typical baffle silencers inserted in an infinite rectangular duct with rigid walls, as shown in Fig. 1. This is done for the sake of increasing clarity, as the extension of the model to tackle more complex situations is demonstrated in Section 4. In the present configuration, three separate domains are defined. In domain I (inlet duct), an incident sound wave propagates in the positive z-direction and excites the silencer. Domain II is the silencer section made up of an arbitrary number N of layers. Airways and baffles can be represented by several layers of length L and height h_j, and can also be separated by a screen (e.g. thin veil or perforated plate). Each baffle contains a bulk reacting porous material, assumed to be both homogeneous and isotropic. Finally, the effect of a metallic fairing or a perforated screen at either end of a baffle is considered. The domain III (outlet duct) represents an anechoic termination. It should be noted that the geometry is invariant along the y-direction.

2.1 Governing equations

Assuming a time dependence of the form $\mathrm{e}^{-\mathrm{i}\omega t}$, the propagation equations for the inlet duct, the outlet duct and the silencer section, can be found in each layer j ($j = 1, \cdots, N$) using continuity and momentum equations:

$$\mathrm{i}\omega\kappa_j p_j = \nabla\cdot\mathbf{v}_j, \tag{1}$$

$$\mathrm{i}\omega\rho_j \mathbf{v}_j = \nabla p_j, \tag{2}$$

where p_j and $\mathbf{v}_j$ are the acoustic pressure and velocity vector. Quantities κ_j and ρ_j are the compressibility and the density of the medium in layer j respectively. In the airways, the fluid is characterized by air compressibility κ_0 and density ρ_0. In the baffles, the fibrous material is described as an equivalent fluid using the limp frame model defined in Appendix A. This model gives better results than rigid frame equivalent models, without the additional computational effort that Biot's model would require [14, 15, 16]. It is based on the assumption that the frame has no bulk stiffness, which is relevant for the mineral wool used in HVAC silencers. Note that other equivalent fluid models can be used, especially if only the air resistivity of the fibrous material is known [17]. The porous medium is characterized by an effective compressibility κ_{eq} and density ρ_ℓ which are frequency-dependent. These effective quantities are recalled in Appendix A.

At this point, the problem is assumed to be two-dimensional which signifies that there is no variation of pressure or velocity along the y-axis. We can therefore express $\mathbf{v}_j$ in terms of the transverse and axial velocity as $\mathbf{v}_j = (v_j, 0, u_j)$. As the airflow Mach number in HVAC systems does not usually exceed 0.05, its effect on the silencer performance is neglected. The averaged propagation equations are obtained following a similar process described by Aurégan *et al.* [13]. By defining the mean pressure $\overline{P}_j$ and the acoustic volume velocity U_j over the height h_j, we obtain the following after integration:

$$Y_j\overline{P}_j = (V_j - V_{j-1}) + \frac{\mathrm{d}U_j}{\mathrm{d}z}, \tag{3}$$

$$Z_j U_j = \frac{\mathrm{d}\overline{P}_j}{\mathrm{d}z}, \tag{4}$$

where $Y_j = \mathrm{i}\omega\kappa_j h_j$ is homogeneous for an admittance per unit area and $Z_j = \mathrm{i}\omega\rho_j/h_j$ is homogeneous for an impedance per unit area. Here, the term V_j is the transverse velocity at the interface x_j as shown in Fig. 2. This quantity is continuous across the interface so we have $V_j = v_j(x_j) = v_{j+1}(x_j)$ (note the z-dependence is omitted here for clarity). Combining Eq. (3) and Eq. (4) yields

$$\left(-\frac{\mathrm{d}^2}{\mathrm{d}z^2} + \Gamma_j\right)\overline{P}_j = Z_j(V_j - V_{j-1}) \tag{5}$$

where $\Gamma_j = Z_j Y_j$. Now, in order to form an eigenvalue problem for the mean pressure, the transverse velocity in Eq. (5) must be expressed in terms of the mean pressure in each layer. This can be done by first assuming that the transverse velocity across the layer j can be fairly well approximated by the piecewise linear function

$$v_j(x) = N_1(x)V_{j-1} + N_2(x)V_j, \tag{6}$$

where the shape functions N_1 and N_2 are the classical linear Lagrange interpolating polynomials

$$N_1(x) = \frac{x_j - x}{h_j} \quad \text{and} \quad N_2(x) = \frac{x - x_{j-1}}{h_j}. \tag{7}$$

Once again we omit the z-dependence for the demonstration. After integrating the momentum equation (2), we obtain

$$p_j(x) = \overline{P}_j + H_j\left[\left(3[N_2(x)]^2 - 1\right)V_j - \left(3[N_1(x)]^2 - 1\right)V_{j-1}\right], \tag{8}$$

where $H_j = \mathrm{i}\omega\rho_j h_j/6$ is homogeneous for an impedance. To account for the presence of an acoustic screen with surface impedance Z_s between the layers j and $j+1$ we require that $Z_s V_j = p_{j+1}(x_j) - p_j(x_j)$. This yields the following linear relation:

$$H_j V_{j-1} + G_j V_j + H_{j+1}V_{j+1} = \overline{P}_{j+1} - \overline{P}_j, \tag{9}$$

with $G_j = Z_s + 2(H_{j+1} + H_j)$. Using the rigid wall conditions $V_0 = V_N = 0$, Eq. (9) can be expressed in the matrix form:

$$\begin{pmatrix} G_1 & H_2 & & & & & \\ H_2 & \ddots & \ddots & & & \mathbf{0} & \\ & \ddots & \ddots & \ddots & & & \\ & & H_j & G_j & H_{j+1} & & \\ & & & \ddots & \ddots & \ddots & \\ & \mathbf{0} & & & \ddots & \ddots & H_{N-1} \\ & & & & & H_{N-1} & G_{N-1} \end{pmatrix} \begin{pmatrix} V_1 \\ V_2 \\ \vdots \\ V_j \\ \vdots \\ V_{N-1} \end{pmatrix} = \begin{pmatrix} \overline{P}_2 - \overline{P}_1 \\ \overline{P}_3 - \overline{P}_2 \\ \vdots \\ \overline{P}_{j+1} - \overline{P}_j \\ \vdots \\ \overline{P}_N - \overline{P}_{N-1} \end{pmatrix}, \tag{10}$$

After inversion, this yields

$$V_j = \sum_{l=1}^{N-1} c_{j,l}\left(\overline{P}_{l+1} - \overline{P}_l\right) \tag{11}$$

and therefore

$$V_j - V_{j-1} = \sum_{l=1}^{N-1} b_{j,l}\overline{P}_l, \tag{12}$$

where

$$b_{j,l} = (\mathbf{B})_{jl} = c_{j,l} + c_{j-1,l-1} - c_{j,l-1} - c_{j-1,l}\,, \tag{13}$$

with the convention that $c_{j,0} = c_{j,N} = 0$. Now, by introducing the mean pressure vector $\overline{\mathbf{P}} = (\overline{P}_1, \cdots, \overline{P}_j, \cdots, \overline{P}_N)^{\mathrm{T}}$, Eq. (5) can be recast into the matrix form

$$\left(-\frac{\mathrm{d}^2}{\mathrm{d}z^2} + \mathbf{\Gamma} + \mathbf{ZB}\right)\overline{\mathbf{P}} = 0, \tag{14}$$

where $\mathbf{Z} = \mathrm{diag}(Z_1, \cdots, Z_j, \cdots, Z_N)$ is the diagonal matrix containing the impedance per area of each layer and $\mathbf{\Gamma} = \mathrm{diag}(\Gamma_1, \cdots, \Gamma_j, \cdots, \Gamma_N)$. Eq. (14) can be interpreted as a 'multi-layered' propagator

for the mean pressure field in the duct and is a key result of this paper. Although this layered model seems somewhat superfluous in the empty part of the duct (domains I and III), it is advantageous to artificially extend the same layered decomposition in these regions as it considerably facilitates the matching conditions, as shown in the next sections.

2.2 Modal decomposition

In each domain $d = \mathrm{I}$, II and III, the mean pressure field $\overline{\mathbf{P}}^d$ may be expanded via the modal decomposition in forward and backward traveling waves

$$\overline{\mathbf{P}}^d(z) = \mathbf{\Phi}^d \left(\mathbf{E}^d(z)\mathbf{A}^{d,+} + \hat{\mathbf{E}}^d(z)\mathbf{A}^{d,-} \right), \tag{15}$$

where the column vector $\mathbf{A}^{d,\pm} = (A_1^{d,\pm}, A_2^{d,\pm}, \cdots, A_M^{d,\pm})^{\mathrm{T}}$ contains the modal amplitudes, the diagonal matrix $\mathbf{E}^d(z)$, and its inverse $\hat{\mathbf{E}}^d(z)$, contains the propagation factors:

$$\mathbf{E}^d(z) = \mathrm{diag}(\mathrm{e}^{\mathrm{i}k_1^d z}, \mathrm{e}^{\mathrm{i}k_2^d z}, \cdots, \mathrm{e}^{\mathrm{i}k_M^d z}), \tag{16}$$

$$\hat{\mathbf{E}}^d(z) = \mathrm{diag}(\mathrm{e}^{-\mathrm{i}k_1^d z}, \mathrm{e}^{-\mathrm{i}k_2^d z}, \cdots, \mathrm{e}^{-\mathrm{i}k_M^d z}). \tag{17}$$

and the matrix $\mathbf{\Phi}^d = (\mathbf{\Phi}_1^d, \mathbf{\Phi}_2^d, \cdots, \mathbf{\Phi}_M^d)$ contains the transverse eigenvectors satisfying the symmetric eigenvalue problem (see $(\mathbf{Z}^d)^{-1}\times$ Eq. (14))

$$\left((\mathbf{Z}^d)^{-1}\mathbf{\Gamma}^d + \mathbf{B}^d\right)\mathbf{\Phi}^d = -(\mathbf{Z}^d)^{-1}\mathbf{\Phi}^d(\mathbf{k}^d)^2, \tag{18}$$

with $\mathbf{k}^d = \mathrm{diag}(k_1^d, k_2^d, \cdots, k_M^d)$ the diagonal matrix containing the axial wavenumbers and M is the number of modes taken into account in the numerical model. It should be noted that generally, the number of modes is equal to the number of layers, although this condition can be relaxed, while in all cases we must have $M \leq N$. Similarly, using Eq. (4), the axial volume velocity is given by the modal expansion

$$\mathbf{U}^d(z) = \mathrm{i}(\mathbf{Z}^d)^{-1}\mathbf{\Phi}^d\mathbf{k}^d \left(\mathbf{E}^d(z)\mathbf{A}^{d,+} - \hat{\mathbf{E}}^d(z)\mathbf{A}^{d,-} \right). \tag{19}$$

The modal amplitudes remain to be determined in order to fully describe the mean pressure field. This last step is performed by applying the axial matching conditions.

2.3 Mode matching

The matching conditions must be satisfied at the interfaces between each domain. Both interfaces $\mathbf{\Sigma}_1$ and $\mathbf{\Sigma}_2$, shown in Fig. 1, comprise three kinds of surface: an impervious surface $\mathbf{\Sigma}^f$ accounting for metallic fairings, a porous surface $\mathbf{\Sigma}^s$ accounting for the presence of an acoustic screen and an open surface $\mathbf{\Sigma}^a$. For instance, on the interface $\mathbf{\Sigma}_1$, we have

- on $\mathbf{\Sigma}_1^a$, the continuity of mean pressure and the volume velocity yields

$$\mathbf{D}_{\mathrm{a}}\overline{\mathbf{P}}^{\mathrm{I}} = \mathbf{D}_{\mathrm{a}}\overline{\mathbf{P}}^{\mathrm{II}}, \tag{20a}$$

$$\mathbf{D}_{\mathrm{a}}\mathbf{U}^{\mathrm{I}} = \mathbf{D}_{\mathrm{a}}\mathbf{U}^{\mathrm{II}}. \tag{20b}$$

- on $\mathbf{\Sigma}_1^f$, the kinematic conditions give

$$\mathbf{D}_f\mathbf{U}^{\mathrm{I}} = 0, \tag{21a}$$

$$\mathbf{D}_f\mathbf{U}^{\mathrm{II}} = 0. \tag{21b}$$

- on $\mathbf{\Sigma}_1^s$, the mean pressure jump with impedance surface Z_s and the continuity of the volume velocity yield

$$Z_s\mathbf{D}_{\mathrm{s}}\mathbf{U}^{\mathrm{I}} = \mathbf{D}_{\mathrm{s}}\left(\overline{\mathbf{P}}^{\mathrm{I}} - \overline{\mathbf{P}}^{\mathrm{II}}\right), \tag{22a}$$

$$\mathbf{D}_{\mathrm{s}}\mathbf{U}^{\mathrm{I}} = \mathbf{D}_{\mathrm{s}}\mathbf{U}^{\mathrm{II}}. \tag{22b}$$

In these equations, we introduced the diagonal matrices $\mathbf{D}_\mathrm{a}, \mathbf{D}_\mathrm{f}$ and $\mathbf{D}_\mathrm{s}$ whose role is to simply select the layer or, equivalently, the lines of the mean pressure vector (and the volume velocity vector) corresponding to the type of surface. For instance, $(\mathbf{D}_\mathrm{a})_{jj} = 1$ if layer j corresponds to an open surface and $(\mathbf{D}_\mathrm{a})_{jj} = 0$ otherwise. In fact, the third scenario on $\mathbf{\Sigma}_1^s$ generalizes the first two cases (Eq. (20a) to Eq. (21b)). This generalized boundary condition is not considered in this paper though its numerical implementation does not present any particular difficulty.

The modal decomposition of the mean pressure and volume velocity (respectively Eq. (15) and Eq. (19)) are substituted into Eq. (20a) to Eq. (21b). Using the same formalism as in [18, 19, 20], this yields the following scattering matrices for both interfaces $\mathbf{\Sigma}_1$ and $\mathbf{\Sigma}_2$:

$$\mathbf{X}_1 \begin{pmatrix} \mathbf{A}^{\mathrm{I},-} \\ \mathbf{A}^{\mathrm{II},+} \end{pmatrix} = \mathbf{Y}_1 \begin{pmatrix} \mathbf{A}^{\mathrm{I},+} \\ \mathbf{A}^{\mathrm{II},-} \end{pmatrix} \quad \text{on } \mathbf{\Sigma}_1, \tag{23a}$$

$$\mathbf{X}_2 \mathbf{E}_X \begin{pmatrix} \mathbf{A}^{\mathrm{II},-} \\ \mathbf{A}^{\mathrm{III},+} \end{pmatrix} = \mathbf{Y}_2 \mathbf{E}_Y \begin{pmatrix} \mathbf{A}^{\mathrm{II},+} \\ \mathbf{A}^{\mathrm{III},-} \end{pmatrix} \quad \text{on } \mathbf{\Sigma}_2, \tag{23b}$$

where $\mathbf{E}_X$ and $\mathbf{E}_Y$ are diagonal matrices containing the propagation factors at $z = L$:

$$\mathbf{E}_X = \mathrm{diag}\left(\hat{\mathbf{E}}^{\mathrm{II}}(L), \mathbf{E}^{\mathrm{III}}(L)\right), \tag{24}$$

$$\mathbf{E}_Y = \mathrm{diag}\left(\mathbf{E}^{\mathrm{II}}(L), \hat{\mathbf{E}}^{\mathrm{III}}(L)\right). \tag{25}$$

The scattering matrices have the following form:

$$\mathbf{X}_1 = \begin{pmatrix} \mathbf{R}^{\mathrm{I}} & -\mathbf{R}^{\mathrm{II}} \\ \mathbf{S}^{\mathrm{I}} & \mathbf{S}^{\mathrm{II}} \\ \mathbf{T}^{\mathrm{I}} & \mathbf{0} \\ \mathbf{0} & \mathbf{T}^{\mathrm{II}} \end{pmatrix}, \quad \mathbf{Y}_1 = \begin{pmatrix} -\mathbf{R}^{\mathrm{I}} & \mathbf{R}^{\mathrm{II}} \\ \mathbf{S}^{\mathrm{I}} & \mathbf{S}^{\mathrm{II}} \\ \mathbf{T}^{\mathrm{I}} & \mathbf{0} \\ \mathbf{0} & \mathbf{T}^{\mathrm{II}} \end{pmatrix}, \tag{26}$$

$$\mathbf{X}_2 = \begin{pmatrix} \mathbf{R}^{\mathrm{II}} & -\mathbf{R}^{\mathrm{III}} \\ \mathbf{S}^{\mathrm{II}} & \mathbf{S}^{\mathrm{III}} \\ \mathbf{T}^{\mathrm{II}} & \mathbf{0} \\ \mathbf{0} & \mathbf{T}^{\mathrm{III}} \end{pmatrix}, \quad \mathbf{Y}_2 = \begin{pmatrix} -\mathbf{R}^{\mathrm{II}} & \mathbf{R}^{\mathrm{III}} \\ \mathbf{S}^{\mathrm{II}} & \mathbf{S}^{\mathrm{III}} \\ \mathbf{T}^{\mathrm{II}} & \mathbf{0} \\ \mathbf{0} & \mathbf{T}^{\mathrm{III}} \end{pmatrix}, \tag{27}$$

where block matrices $\mathbf{R}^d$ and $\mathbf{S}^d$ are of the same size, i.e. $N_a \times M$ whereas the block matrix $\mathbf{T}^d$ which corresponds to the hard wall condition on the metallic fairing is of size $N_f \times M$:

$$\mathbf{R}^d = \mathbf{D}_\mathrm{a} \mathbf{\Phi}^d, \tag{28}$$

$$\mathbf{S}^d = \mathbf{D}_\mathrm{a} \left(\mathbf{Z}^d\right)^{-1} \mathbf{\Phi}^d \mathbf{k}^d, \tag{29}$$

$$\mathbf{T}^d = \mathbf{D}_\mathrm{f} \mathbf{\Phi}^d \mathbf{k}^d. \tag{30}$$

The number of lines, N_a and N_f, corresponds to the total number of layers for the airways and for the metallic fairings, respectively, thus $N_a + N_f = N$. At this point, it is worth mentioning that scattering matrices are formed simply, algebraically, at almost no cost once the duct acoustic modes contained in $\mathbf{\Phi}^d$ have been found. This is a considerable simplification when compared to more classical mode matching techniques (usually using collocation or weighted residual formulations) encountered in the literature [21, 12, 20, 22]. From then on, and in order to simplify the analysis, the number of modes M is chosen equal to the number of layers N in our calculations.

The overall system is then solved iteratively [18] for the modal amplitudes. The incident modal amplitude, $\mathbf{A}^{\mathrm{I},+}$, is set according to the source characteristics. Initially $\mathbf{A}^{\mathrm{II},-}$ is fixed at zero. The system (23a) is then inverted and generates an initial value for the modal amplitudes oriented rightwards $\mathbf{A}^{\mathrm{II},+}$. This value is then used to solve the system (23b) at the outlet plane for an initial value of $\mathbf{A}^{\mathrm{III},+}$. The process is then reiterated until the modal amplitudes show a sufficiently small change (less than 10^{-6}) in the successive iteration cycles. More complex situations involving more than three domains (this happens if baffles are misaligned for instance) can be dealt with following the same principle.

The performances of the baffle-type silencer are usually measured via the Transmission Loss (TL) which is defined as the ratio of the incident to transmitted sound powers. The incident sound power

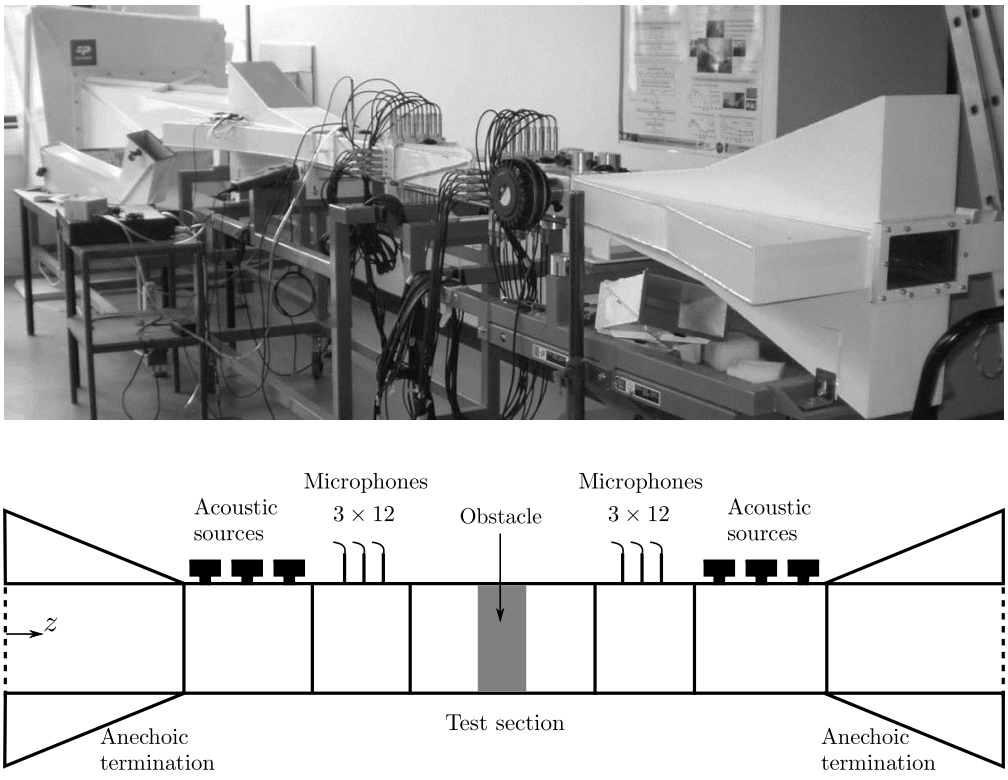

Figure 3: Multimodal UTC test bench [23] - 72 microphones for 10 modes resolution.

may be taken equal to unity without any loss of generality. In the domain III the eigenvalue problem (see Eq. (18)) involves Hermitian and positive-definite matrices. The corresponding transverse eigenvectors are pairwise orthogonal according to $(\mathbf{\Phi}^{\mathrm{III}})^{\mathrm{T}}(\mathbf{Z}^{\mathrm{III}})^{-1}\mathbf{\Phi}^{\mathrm{III}} = \mathbf{I}$, with $\mathbf{I}$ the identity matrix. After integration over the cross-section, the transmitted sound power can write:

$$\begin{aligned} \mathrm{W}_{\mathrm{tr}} &= \frac{1}{2}\mathrm{Re}\left(\overline{\mathbf{P}}^{\mathrm{III}}\left(\mathbf{U}^{\mathrm{III}}\right)^{\dagger}\right) \\ &= \frac{1}{2}(\mathbf{A}^{\mathrm{III},+})^{\dagger}(\mathbf{k}^{\mathrm{III}})^{\dagger}\mathbf{A}^{\mathrm{III},+}, \end{aligned} \tag{31}$$

where † is the Hermitian transpose. Hence, per unit length in the y-direction and in decibels (dB)

$$\mathrm{TL} = -10\,\log_{10}\left(\frac{1}{2}\sum_{n=1}^{M_p} k_n^{\mathrm{III}}|A_n^{\mathrm{III},+}|^2\right), \tag{32}$$

where M_p is the number of propagating modes in the outlet duct, i.e. k_n^{III} is a real number.

3 Results and validation for symmetrical silencers with periodic arrangements

In order to assess the robustness of the method proposed, simulated results for two silencers presenting symmetry and with periodic baffle arrangements (see Figs. 4(a)) and 4(b)) are compared with measurements carried out by the authors in our laboratory. It should be noted that for such silencers, very few narrow band experimental data giving access to higher mode contributions are available in the literature [6]. Indeed, most of them are octave-band [5] or one-third octave-band [10] data. The test bench and the geometry of the silencers are described first.

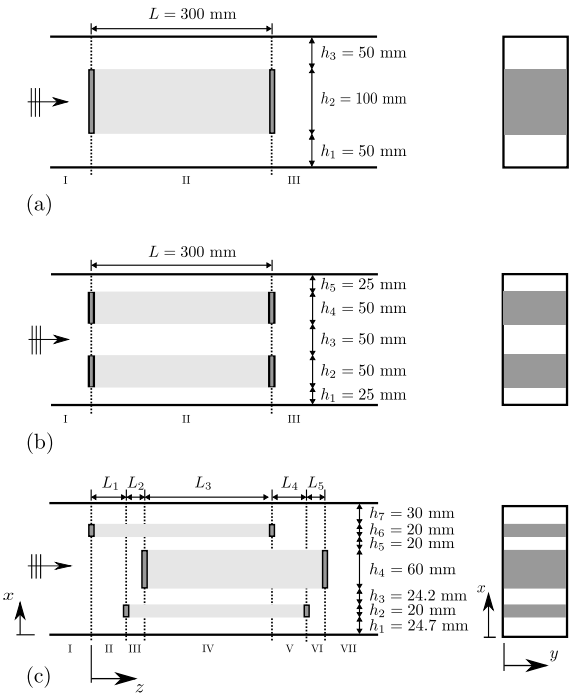

Figure 4: Plan view (left) of the geometry for (a) one-baffle silencer: silencer A, (b) a two-baffle silencer: silencer B and (c) a three-baffle silencer: silencer C. Cross-section view (right).

3.1 Test bench and experimental procedure

The measurements were performed on a test bench (Fig. 3) designed for the multimodal characterization of the acoustic properties of obstacles (the dissipative silencer is considered as an obstacle in this context) in the presence (or not) of a low Mach number flow [23]. The duct facility is a rigid rectangular duct of 0.2 m $\times$ 0.1 m section with an anechoic termination at either end. The results are given within the frequency band [200 Hz - 3.5 kHz] which limits the number of propagative modes in the duct to a maximum of $M_s = 10$. The $2M_s$-port scattering matrix, which contains the modal reflection and transmission coefficients, is measured using a multi-source method described in [23].

The experimental procedure is carried out for silencer A (Fig. 4(a)) and silencer B (Fig. 4(b)). These two silencers have the same length and are inserted in a duct with the same cross-sectional area. Silencer A consists of one baffle 100 mm thick whereas silencer B consists of two baffles both of which are 50 mm thick. RW mineral wool was chosen to fill the baffles. Its properties were determined by measurements carried out by the authors and given in Table 1. Both silencers have the same open area ratio equal to 50%. They were chosen in this way to investigate the effect of the number of baffles on the silencer's performances while keeping the same area ratio for the airway. In the airway, the density and the speed of sound are respectively $\rho_0 = 1.2$ kg.m^{-3} and $c_0 = 342.8$ m.s^{-1}. The values for the duct cut-off frequencies are recalled below:

$$f_{(n,m)} = \frac{c_0}{2}\sqrt{\left(\frac{n}{0.2}\right)^2 + \left(\frac{m}{0.1}\right)^2}. \tag{33}$$

For an incident plane wave, it is clear for reasons of invariance in the y-direction that only transverse modes in the x-direction are generated. The cut-off frequencies of interest are thus: $f_{(1,0)} = 857$ Hz, $f_{(2,0)} = 1714$ Hz, $f_{(3,0)} = 2571$ Hz, $f_{(4,0)} = 3428$ Hz and $f_{(6,0)} = 5130$ Hz.

3.2 Results

The results are given here for a plane wave excitation. Silencer A comprised three layers (two airways and one baffle) so it was natural to apply our model with $N = 3$. The corresponding Transmission Loss is shown in Fig. 5 as is the measured TL. Good agreement can be seen in the low part of the

Table 1: Material properties for the RW mineral wool.

ϕ	σ	α_∞	Λ	Λ'	ρ_1
–	(N.s.m^{-4})	–	(μm)	(μm)	(kg.m^{-3})
0.954	14066	1	91.2	182.4	53

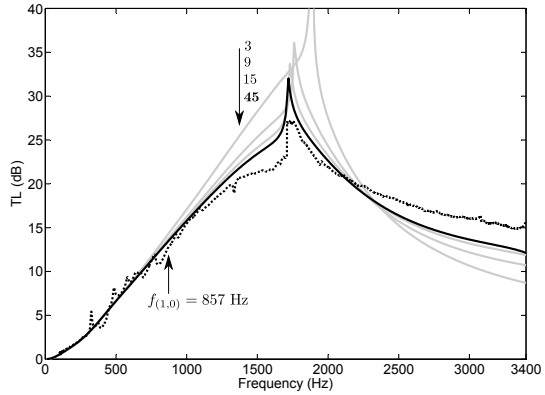

Figure 5: Convergence of predicted TL for plane wave excitation with respect to the total number of layer N for the silencer A, — $N = 3$, 9 and 15, — $N = 45$, ··· measurements.

spectrum (below the first cut-off frequency, i.e. 857 Hz). Above this frequency, the 3-layer model was too coarse and could not correctly simulate higher-order modes or capture the scattering mechanisms occurring at the junctions $\mathbf{\Sigma}_1$ and $\mathbf{\Sigma}_2$ especially around certain cut-off frequencies.

To remedy this, each layer was subdivided into sublayers in order to refine the model. A convergence analysis is shown in Fig. 5 by taking successively 3, 9 (3 subdivisions), 15 (5 subdivisions) and 45 (15 subdivisions) for the total number of layers N. The results obtained with $N = 45$ layers converged though $N = 15$ is sufficient to ensure reasonable values for engineering purposes. It should be noted that these results were computed with modest computational effort: it took only about 4 seconds (4 iterations per frequency step) using Matlab to compute 340 frequencies with the refined model, $N = 15$ layers, on a laptop computer.

The same analysis was conducted for silencer B and the results are shown in Fig. 6. Good agreement with the measurements are found in both cases and the results indicate that the noise reduction performances are quite different. Indeed, for silencer A, the peak at 1714 Hz corresponding to the cut-off frequency of the first transverse symmetric mode (2,0) is clearly identified both experimentally and numerically. For silencer B, only a continuous increase of the TL is observed and discrepancies do not exceed 3 dB even when using only $N = 5$ layers. The presence of three small peaks at 325 Hz, 486 Hz and 583 Hz are caused by the vibration of the duct wall [23].

The magnitudes of the reflection and transmission coefficients for silencer A are compared with measurements in Fig. 7. It can be seen that only the fundamental and the first transverse symmetric modes are shown as the contribution from the other modes is negligible. In fact silencer A behaves as an acoustic filter for the odd modes; the reasons for this are explained briefly in the next section.

4 Analysis and discussion

4.1 Analysis of Transmission Loss

In this subsection, the performances of silencers A and B are discussed first. More complex configurations involving non-periodic and misaligned silencers are then considered and analyzed.

Predicted performances for an incident plane wave mode are reported (in black lines) in Fig. 8 up to 5 kHz for silencers A and B. The difference in performance depends on the position of a maximum peak corresponding to the cut-off frequency of the first transverse symmetrical mode (2,0) for silencer A and to the mode (4,0) for silencer B. Above this frequency, the TL decreases steadily. This behavior

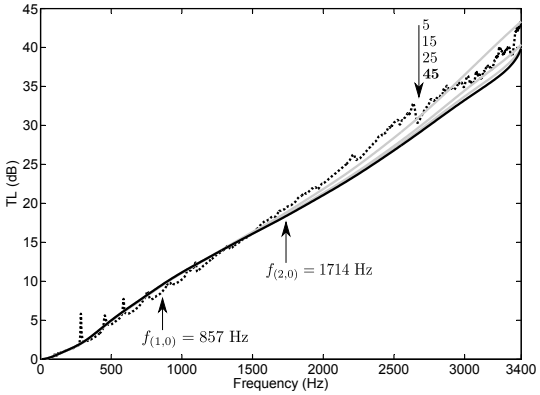

Figure 6: Convergence of predicted TL for plane wave excitation with respect to the total number of layers N for silencer B, ——— $N = 5$, 15 and 25, ——— $N = 45$, · · · measurements.

is typical of a periodic and symmetrical silencer. Indeed, it can be shown in this very particular case that the modes transmitted satisfy the selection rule [9]

$$n = n^{inc} + 2qK. \tag{34}$$

Here, n^{inc} is the order of the incident mode (which is zero here as only the plane wave mode is considered), K is the number of baffles and q is an integer. In the case of silencer A, for instance, $K = 1$ and only even modes are allowed to propagate. It can be noted that this could have been anticipated using symmetry arguments. For silencer B, however, the selection rule indicates that only modes of order $n = 4q$ are allowed, the other modes being forbidden. When the frequency exceeds the cut-off frequency of the selected mode, the latter is strongly coupled with higher modes in the silencer section and is likely to carry a substantial amount of acoustic energy (this energy could not be radiated below cut-off). This new contribution necessarily implies a reduction in TL and poorer performances. Fig. 9 typically illustrates the acoustic pressure field in both silencers. It shows the absence of mode coupling with the mode (2,0) for silencer B.

In order to examine the effects of asymmetry in the spatial arrangement of the baffles: the two baffles of silencer B were shifted to the bottom (in the x-direction). In the first scenario, we took $h_1 = 12.5$ mm and $h_1 = 0$ mm for the second configuration (see Fig. 4). The TL are shown in Fig. 8. These configurations are no longer symmetrical and in both cases, all modes are allowed to radiate. This yields poorer performances beyond the cut-off frequency of the first symmetric mode (2,0) as well as a smoothing of the TL curves around the peak. Note also that the second configuration shows a slight improvement of the performances below this frequency.

To push the analysis one step further, the three-baffle silencer C, shown in Fig. 4(c), is now investigated. Two scenarios are considered: the first corresponds to a conventional arrangement $L_1 = L_2 = 0$ and in the second scenario, two baffles have been shifted along the axial direction with $L_1 = 53.5$ mm and $L_2 = 19$ mm. In the latter case, there are seven domains and therefore six junctions for each of which a scattering matrix must be calculated. In order to give a fair comparison, the open area ratio and the length of the baffles are identical to those of silencers A and B. The results are shown in Fig. 10. The dark dashed curve corresponds to a standard three-baffle silencer, i.e. symmetrical and periodic. In the low frequency regime, before the first cut-off frequency, all three-baffle silencers give the same performances whereas in the medium frequency regime, silencer C produces the best results. Above the third cut-off frequency, the standard three-baffle silencer performs better. The effect of shifting the baffles axially is only visible in the high frequency range. This is partly due to the fact that the mode (6,0) is less excited and the acoustic power transmitted is reduced, showing a difference of nearly 8 dB in noise reduction. This illustrative example shows that the performance of parallel baffle-type silencers also depends on their geometrical configurations (namely the height of each baffle as well as their positions) and can be tailored to meet specific noise reduction targets. Silencer C, for instance, appears to be a good trade-off between the one-baffle and the three-baffle silencers.

Finally, the effect of a resistive screen is investigated. The presence of a resistive screen between each layer of air and fibrous material can be easily taken into account in the numerical model. It is

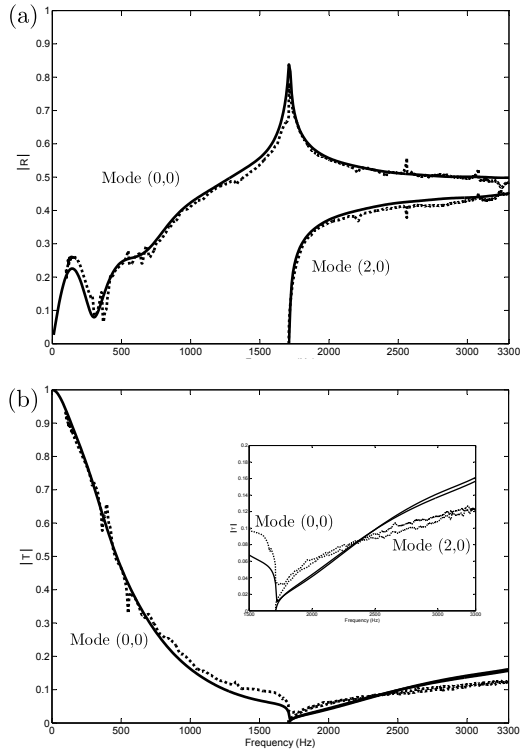

Figure 7: Magnitude of the modal reflection coefficients (a) and transmission coefficients (b) for an incident plane wave for the silencer A. ——— Numerical results, · · · measurements.

sufficient to modify the parameter $G_j = Z_s + 2(H_{j+1} + H_j)$ in Eq. (9) accordingly. To make things simpler, we consider the same screen for all the interfaces and, neglecting the reactance part, the impedance is given by the classical formula $Z_s = \sigma_s d$ where σ_s is the resistivity and d the screen thickness. Fig. 11 shows the influence of the resistivity on the performances of silencer B. As long as σ_s remains below that of the absorbing material, there is no visible effect on the TL curve. However, for higher values, i.e. $\sigma_s = 200$ kN.s.m^{-4} and 500 kN.s.m^{-4}, a secondary peak appears. This is the result of a resonant effect within the baffle induced by the resistive screen. Finally, as resistivity increases the screen acts as a rigid wall and the shape of the TL curve resembles that of a purely reactive expansion chamber.

4.2 Analysis in terms of acoustic power

The performance of symmetrical and periodic parallel-baffle silencers is now discussed using power balance. The energy conservation condition implies that the incident sound power is equal to the sum of the reflected, dissipated and transmitted sound powers. The evolution of the reflected, transmitted and dissipated sound powers is then examined as a function of the frequency in Fig. 12 for both silencers A and B. It can be seen that three regimes stand out: (i) dissipation increases sharply until reflection becomes higher than transmission; (ii) reflection increases to the detriment of dissipation, while transmission keeps decreasing until it reaches nearly zero at the cut-on of the mode (2,0) for silencer A and (4,0) for silencer B; (iii) finally, the transmitted sound power starts increasing slowly once the selected mode (2,0) (or (4,0)) becomes propagative. This occurs at the cost of the reflected sound powers. These three regimes allow interpreting the different slopes of the TL.

4.3 Low frequency approximation

The evolution of sound powers for silencers A and B, show that dissipation prevails until reflection becomes higher than transmission (first regime). Therefore silencer performance is almost entirely due

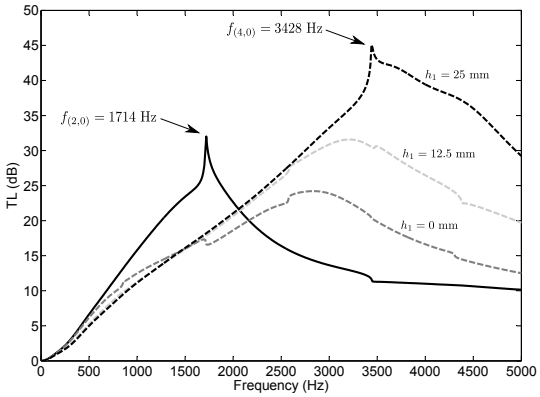

Figure 8: Predicted transmission loss for plane wave excitation with $N = 45$; ——— silencer A, - - - silencer B ($(h_1, h_5) = (25$ mm, 25 mm$)$), - - - silencer B for $(h_1, h_5) = (12.5$ mm, 37.5 mm$)$ and - - - $(h_1, h_5) = (0$ mm, 50 mm$)$.

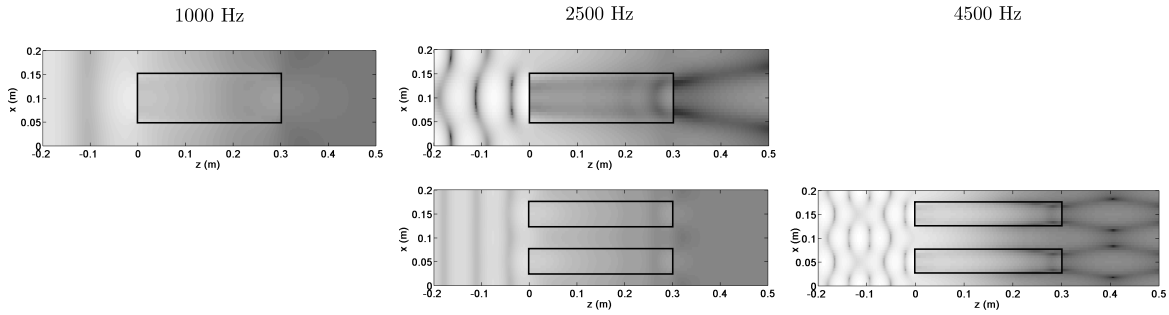

Figure 9: Sound pressure reconstruction, using the scheme presented, at 1000 Hz and 2500 Hz for silencer A (top), and at 2500 Hz and 4500 Hz for silencer B (bottom); here the minimum of the normed pressure field is in black.

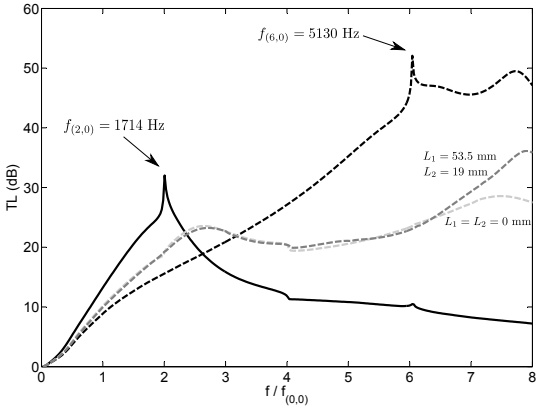

Figure 10: Predicted transmission loss for plane wave excitation. ——— Silencer A; - - - standard three-baffles silencer; - - - silencer C with $(L_1, L_2) = (0$ mm$, 0$ mm$)$; - - - silencer C with $(L_1, L_2) = (53.5$ mm$, 19$ mm$)$.

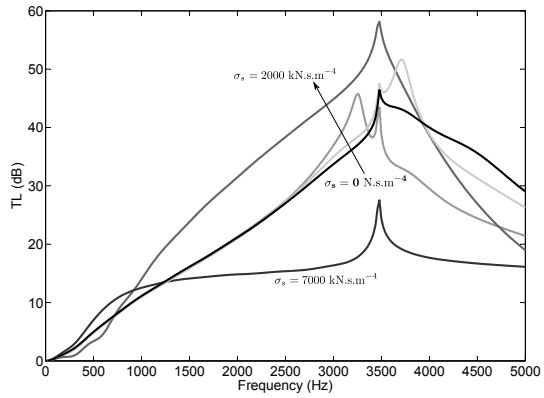

Figure 11: Predicted transmission loss for silencer B with a 0.3 mm thick resistive screen of resistivity σ_s between each layer of air and fibrous material, for plane wave excitation, with $N = 25$; the black line for silencer B for $\sigma_s = 0$ N.s.m^{-4}, in grey lines from light to dark, for silencer B for $\sigma_s = 200, 500, 2000$ and 7000 kN.s.m^{-4}.

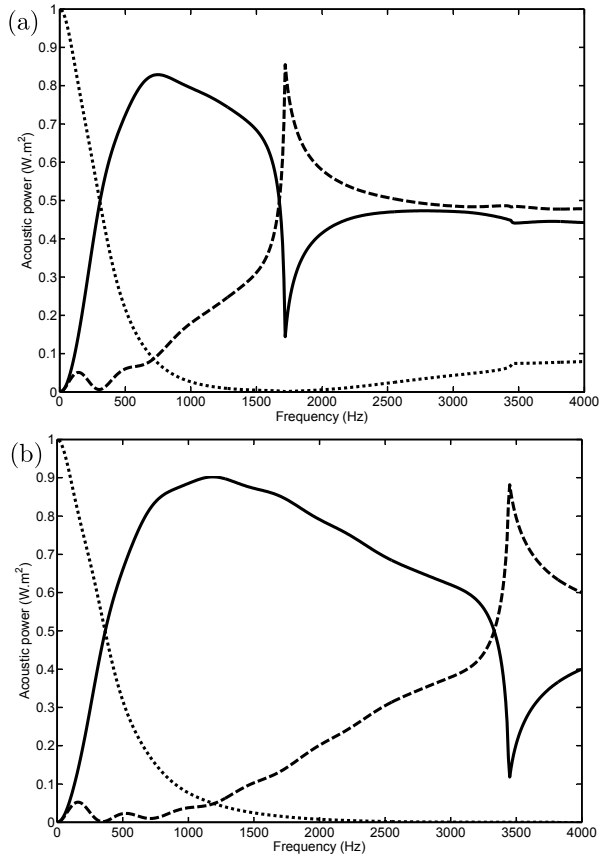

Figure 12: Evolution of the sound powers: (a) silencer A, (b) silencer B; ——— dissipated sound power, – – – reflected sound power, · · · transmitted sound power.

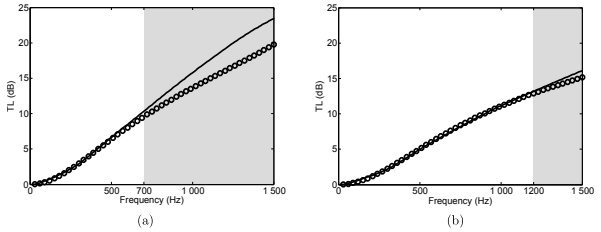

Figure 13: Numerical transmission loss and analytical attenuation for plane wave excitation with symmetrical geometries; — numerical TL and ∘ analytical attenuation. (a) silencer A, (b) silencer B.

to dissipative effects. We show here that at low frequencies the TL of symmetrical silencers, with periodic arrangement of the baffles, can be approximated by determining only the attenuation in the silencer section.

This periodic arrangement of the baffles allows obtaining a simplified equivalent geometry of the silencer by taking into account the different symmetries [10]. Thus for silencers A and B, the equivalent geometry is made up of two layers: one airway and one baffle of height h_1. The two axial wavenumbers k_1 and k_2 in the silencer section are then determined using the model presented above. The final eigenvalue problem can be solved analytically as described in Appendix B. The attenuation of the silencer is finally given by the least attenuated mode [9]:

$$\text{Att} = 8.686\ \text{Im}(k_1)L. \tag{35}$$

Comparison between numerical TL and analytical attenuation is shown in Fig. 13 for silencers A and B. Good agreement is found in both cases up to a limit frequency above which reflection becomes higher than transmission (grey zones). For silencers A and B the limit frequency is respectively 700 Hz and 1200 Hz.

5 Conclusion

In this paper, we presented a two-dimensional multimodal model for the simulation of acoustic propagation through parallel-baffle silencers. The numerical model relies mainly on the computation of approximate acoustic modes for the mean pressure in each layer corresponding either to the airway or the baffle. In this respect, it bears some resemblance with classical FEM as each layer or sublayer can be viewed as a constant element approximation with the subtle difference that the degrees of freedom are not the nodal values of the pressure but its average value across the layer. The method offers the advantage that it greatly simplifies the mode matching procedure at the junction between successive domains and it can be used to tackle relatively complex geometrical configurations with the possibility of taking into account the presence of resistive screens between the porous baffle and the air domain. It is also an easy-to-implement and relatively inexpensive model suitable for optimization purposes.

For a plane wave excitation, comparisons with experimental data were carried out by the authors for two standard configurations: a one parallel-baffle silencer and a two parallel-baffle silencer with the same open area ratio. Good agreement was found in both cases even in the vicinity of the peaks in the TL curves.

More complex configurations were simulated in order to examine the influence of silencer symmetry and periodicity on the modal coupling and acoustic performances. Investigations were conducted by varying the number of baffles, the height of each baffle and their relative positions along both the axial and transverse directions. The impact due to the presence of resistive screens on noise reduction was also examined. Although symmetrical and periodic configurations provide very good performances it was shown that more complex configurations can be useful in order to meet specific noise reduction targets. A low-frequency analytical model was developed to determine the axial wavenumbers of silencers with periodic baffle arrangements. It was shown that, up to a limit frequency, it is possible to approximate transmission loss accurately. This analytical model can be used as a preliminary design tool for parallel baffle silencers.

Work is ongoing by the authors to develop optimization procedures for larger size systems, based on a selected number of design parameters (height, position and material properties) and more complex configurations which accentuate the reactive behaviour of the silencer with resonant cavities.

Acknowledgement

The authors would like to thank the ANRT (Association Nationale de la Recherche et de la Technologie) for their financial support.

Appendix A: the limp frame model

The limp frame model [14, 15, 16] assumes that the bulk stiffness of the porous skeleton is neglected. Sound propagation can be characterized by an effective compressibility κ_{eq} and density ρ_ℓ, which are complex-valued and frequency dependent. As in the rigid frame model [17], the compressibility of the limp model is the modified compressibility of the saturating fluid and is given by

$$\kappa_{eq}(\omega) = \phi\kappa_0 \left(\gamma - \frac{(\gamma-1)}{1 - \frac{8\mu}{\mathrm{i}\omega\rho_0 \mathrm{Pr}\Lambda'^2} G'(\omega)} \right), \tag{36}$$

with

$$G'(\omega) = \sqrt{1 - \mathrm{i}\frac{\omega\rho_0 \mathrm{Pr}\Lambda'^2}{16\mu}}, \tag{37}$$

where ϕ is the porosity, γ the ratio of the specific heats of the air, μ the air viscosity, Pr the Prandlt number and Λ' the thermal characteristic length. The inertia of the solid phase is accounted for in the effective density of the fluid:

$$\rho_\ell(\omega) = \frac{\rho_{eq}(\omega)\rho_t - \rho_0^2}{\rho_t + \rho_{eq}(\omega) - 2\rho_0}, \tag{38}$$

where $\rho_t = \rho_1 + \phi\rho_0$ is the total apparent mass of the equivalent fluid limp medium, ρ_1 is the density of the skeleton and $\rho_{eq}(\omega)$ is the effective density accounting for the rigid frame model given by

$$\rho_{eq}(\omega) = \frac{\alpha_\infty \rho_0}{\phi} \left[1 - \frac{1}{\mathrm{i}\hat{\omega}} G(\omega) \right], \tag{39}$$

with

$$G(\omega) = \sqrt{1 - \mathrm{i}\frac{\hat{M}}{2}\hat{\omega}}. \tag{40}$$

Here, $\hat{\omega} = \frac{\omega\alpha_\infty\rho_0}{\phi\sigma}$ is the dimensionless frequency and $\hat{M} = \frac{8\alpha_\infty\mu}{\phi\Lambda^2\sigma}$ the form factor, where σ is the air flow resistivity, α_∞ the tortuosity and Λ the viscous characteristic length.

Appendix B: analytical axial wavenumbers of silencers with two layers

The method presented in the present paper is applied here for a silencer with two layers which allows the eigenvalue problem to be solved analytically. The results bear resemblances to those of [13] for a coaxial cylindrical dissipative silencer. The equality (9) for the transverse velocity at the air-porous interface $x = x_1 = h_1$ (recall that $x_0 = 0$ and $x_2 = h_x = h_1 + h_2$) is simply

$$G_1 V_1 = \overline{P}_2 - \overline{P}_1, \tag{41}$$

which yields the eigenvalue problem (see Eq. (18)):

$$\begin{pmatrix} \Gamma_1 + \frac{Z_1}{G1} & \frac{-Z_1}{G_1} \\ \\ \frac{-Z_2}{G_1} & \Gamma_2 + \frac{Z_2}{G_1} \end{pmatrix} \begin{pmatrix} \overline{P}_1 \\ \\ \overline{P}_2 \end{pmatrix} = -k^2 \begin{pmatrix} \overline{P}_1 \\ \\ \overline{P}_2 \end{pmatrix}. \tag{42}$$

The eigenequation for the wavenumber becomes:

$$k^4 + \left(\Gamma_1 + \Gamma_2 + \frac{(Z_1 + Z_2)}{G_1}\right) k^2 + \Gamma_1\Gamma_2 + \frac{(\Gamma_1 Z_2 + \Gamma_2 Z_1)}{G_1} = 0. \tag{43}$$

The two wavenumbers are

$$k_1^2 = -\frac{(\Gamma_1 + \Gamma_2)}{2} - \frac{(Z_1 + Z_2)}{2G_1}(1 - A), \tag{44}$$

$$k_2^2 = -\frac{(\Gamma_1 + \Gamma_2)}{2} - \frac{(Z_1 + Z_2)}{2G_1}(1 + A), \tag{45}$$

where

$$A = \sqrt{1 + \frac{(\Gamma_1 - \Gamma_2)G_1}{(Z_1 + Z_2)^2}\left[(\Gamma_1 - \Gamma_2)G_1 + 2(Z_1 - Z_2)\right]}. \tag{46}$$

References

[1] R. J. Astley, A. Cummings, A finite element scheme for attenuation in ducts lined with porous material: comparison with experiment, J. Sound Vib. 116 (2) (1987) 239–263.

[2] K. S. Peat, K. L. Rathi, A finite element analysis of the convected acoustic wave motion in dissipative silencers, J. Sound Vib. 184 (3) (1995) 529–545.

[3] O. Z. Mehdizadeh, M. Paraschivoiu, A three-dimensional finite element approach for predicting the transmission loss in mufflers and silencers with no mean flow, Appl. Acoust. 66 (2005) 902–918.

[4] B. Nennig, M. Ben Tahar, E. Perrey-Debain, A displacement-pressure finite element formulation for analyzing the sound transmission in ducted shear flows with finite poroelastic lining, J. Acoust. Soc. Am. 130 (1) (2011) 42–51.

[5] D. Borelli, C. Schenone, A finite element model to predict sound attenuation in lined and parallel-baffle rectangular ducts, HVAC&R Research 18 (3) (2012) 390–405.

[6] T. W. Wu, C. Y. R. Cheng, P. Zhang, A direct mixed-body boundary element method for packed silencers, J. Acoust. Soc. Am. 111 (6) (2002) 2566–2572.

[7] S.-H. Ko, Theoretical analysis of sound attenuation in acoustically lined flow ducts separated by porous splitters (rectangular, annular and circular ducts), J. Sound Vib. 39 (4) (1975) 471–487.

[8] A. Cummings, N. Sormaz, Acoustic attenuation in dissipative splitter silencers containing mean fluid flow, J. Sound Vib. 168 (2) (1993) 209–227.

[9] F. P. Mechel, Theory of baffle-type silencers, Acustica 70 (1990) 93–111.

[10] F. P. Mechel, Numerical results to the theory of baffle-type silencers, Acustica 72 (1990) 7–20.

[11] K. L. Tam, F. J. Fahy, A theoretical and experimental investigation of sound intensity distribution within a splitter silencer, J. Sound Vib. 151 (2) (1991) 213–246.

[12] R. Kirby, The influence of baffle fairings on the acoustic performance of rectangular splitter silencers, J. Acoust. Soc. Am. 118 (4) (2005) 2302–2312.

[13] Y. Aurégan, A. Debray, R. Starobinski, Low frequency sound propagation in a coaxial cylindrical duct: application to sudden area expansions and to dissipative silencers, J. Sound Vib. 243 (3) (2001) 461–473.

[14] O. Doutres, N. Dauchez, J.-M. Génevaux, O. Dazel, Validity of the limp model for porous materials: a criterion based on the Biot theory, J. Acoust. Soc. Am. 122 (4) (2007) 2038–2048.

[15] R. Panneton, Comments on the limp frame equivalent fluid model for porous media, J. Acoust. Soc. Am. 122 (6) (2007) 217–222.

[16] O. Doutres, N. Dauchez, J.-M. Génevaux, O. Dazel, A frequency independent criterion for describing sound absorbing materials by a limp frame model, Acta Acust. United Ac. 95 (2009) 178–181.

[17] J.-F. Allard, N. Atalla, Propagation of Sound in Porous Media: Modelling Sound Absorbing Materials, 2nd Edition, John Wiley, 2009.

[18] A. Cummings, I.-J. Chang, Sound attenuation of a finite length dissipative flow duct silencer with internal mean flow in the absorbent, J. Sound Vib. 127 (1) (1988) 1–17.

[19] B. Nennig, E. Perrey-Debain, M. Ben Tahar, A mode matching method for modeling dissipative silencers lined with poroelastic materials and containing mean flow, J. Acoust. Soc. Am. 128 (6) (2010) 3308–3320.

[20] G. Gabard, R. J. Astley, A computational mode matching approach for sound propagation in three-dimensional ducts with flow, J. Sound Vib. 315 (2008) 1103–1124.

[21] R. Kirby, J. B. Lawrie, A point collocation approach to modelling large dissipative silencers, J. Sound Vib. 286 (4) (2005) 313–339.

[22] B. Nennig, Y. Renou, J.-P. Groby, Y. Aurégan, A mode matching approach for modeling two dimensional porous grating with infinitely rigid or soft inclusions, J. Acoust. Soc. Am. 131 (5) (2012) 3841–3852.

[23] H. Trabelsi, N. Zerbib, J.-M. Ville, F. Foucart, Passive and active acoustic properties of a diaphragm at low mach number, Eur. J. Comp. Mech. 20 (1-4) (2011) 49–71.